Published in final edited form as:
Biochim Biophys Acta. 2011 March ; 1814(3): 435–448. doi:10.1016/j.bbapap.2011.01.003.

Osmoprotective proteome adjustments in mouse kidney papilla

B. J. Gabert[1] and **D. Kültz**[1,*]

[1] Department of Animal Science, University of California, Davis, One Shields Ave., Davis, CA 95616, USA

Abstract

The papilla of the mammalian kidney must tolerate greatly varying degrees of hyperosmotic stress during urine concentration and depending on whole organism hydration state. To identify proteome adaptations supporting cell function and survival in such a harsh environment we compared the proteome of a) the hyperosmotic renal papilla with that of adjacent iso-osmotic cortex tissue and b) the renal papilla of diuretic versus that of anti-diuretic mice. Though functionally distinct the papilla is in close physical proximity to the renal cortex, an iso-osmotic region. Proteomic differences between the papilla and cortex of C57BL6 mice were identified using two-dimensional gel electrophoresis and MALDI-TOF/TOF mass spectrometry. We found 37 different proteins characteristic of the cortex and 16 proteins over-represented in the papilla. Regional specificity was confirmed by Western Blot and further substantiated by immunohistochemistry for selected proteins. Proteins that are characteristic of the renal papilla include αB crystallin, Hsp beta-1, Hsp90, 14-3-3 protein, glutathione S-transferase, aldose reductase, actin and tropomyosin. Gene ontology analysis confirmed a significant increase in molecular functions associated with protein chaperoning and cell stabilization. Proteins over-represented in the cortex were largely related to routine metabolism. During antidiuresis 15 different proteins changed significantly while 18 different proteins changed significantly during diuresis relative to normally hydrated controls. Changes were confirmed by Western blot for selected proteins. Proteins that are significantly altered by diuretic state are associated with cell structure (actin, tubulin), signaling (Rho GDP dissociation inhibitor, abhydrolase domain-containing protein 14B), chaperone functioning (Hsp beta-1, αB crystallin, T complex protein-1) and anti-oxidant functions (α-enolase, GAPDH and LDH). Taken together our study reveals that specific proteins involved in protein folding, cytoskeletal stabilization, antioxidant responses, and stress signaling contribute greatly to the unique hyperosmotic stress resistant phenotype of the kidney papilla.

Introduction

The kidneys are paired organs that play a vital role in the mammalian urinary system filtering blood and ultimately producing urine. As ultrafiltrate progresses through the ascending limb it is diluted due to solute re-absorption in this water impermeable segment resulting in hypo-osmotic ultrafiltrate leaving the thick ascending limb (TAL). This allows for the generation of dilute urine since, under water loaded conditions, the collecting duct need not alter the composition significantly and the urine produced will be voluminous [1].

*Corresponding author dkueltz@ucdavis.edu.

The nephrons are organized within the gross anatomy such that the glomeruli, the proximal and distal tubules, as well as the initial portion of the collecting duct, are contained within the outer portion of the kidney known as the cortex. This region is iso-osmotic to blood. The inner portion of the kidney, the medulla, houses the Loop of Henle and the collecting duct as well as the vasa recta [1]. This organization has functional importance. The high interstitial osmolality of the medulla is utilized by the collecting duct to generate a driving force for water reabsorption. The papilla is the innermost part of the medulla where urine is transported to the renal pelvis before leaving the kidney via the ureter. It is composed mainly of collecting ducts and is exposed to the highest osmolality within the kidney [2].

Processes of the nephron are dynamic and regulated by many hormones and local factors [1]. The proximal tubule, TAL and collecting duct are under hormonal control. Decreased effective circulating volume (ECV) or increased plasma osmolality stimulate vasopressin which causes increased water reabsorption in the distal tubule and collecting duct via insertion of water channels in the distal tubule and collecting duct. Hormone levels vary to maintain homeostasis leading to production of urine with varying osmolality from <100 mOsm up to several-fold (>3000 mOsm in rodents) the concentration of blood (290 mOsm) [3].

High and variable interstitial osmolality underlie the ability to regulate water and solute balance at the cost of generating an inhospitable environment for cell functioning. Interstitial osmolality is increased by high levels of sodium chloride and urea [2]. Urea can cross the cell membrane relatively easily and inside the cell has a denaturing effect on proteins leading to perturbed function. The high interstitial sodium chloride produces an extracellular environment hypertonic to the cell leading to transient water efflux and cell shrinkage that is counteracted by active inorganic ion uptake. Increased inorganic ions counteract the osmotic imbalance and restore cell volume by causing water to follow passively (osmosis) but cannot serve as a long-term solution due to severe perturbations of protein structure and function [4]. Over time organic osmolytes are accumulated to replace the inorganic ions as they are compatible with proper protein function [5]. Organic osmolytes are molecules normally present as metabolic intermediates. Hyperosmotic stress leads to an increase in organic osmolytes in the form of triethylamines, polyols (e.g. sorbitol) and the amino acid taurine through uptake, production and reduced degradation [6].

A long-standing goal of renal cell physiology is to investigate the mechanisms underlying the high tolerance of renal papillary cells to extreme hyperosmotic stress. Salt and urea levels in the papillary interstitium are highly variable; therefore protective mechanisms must constantly adapt to the severity of the stressor. Much remains unknown concerning how cells perceive changes in their osmotic environment and how renal cells adapt to such changes.

A proteomic approach was chosen to gain insight into adaptive responses of renal papillary cells to hyperosmolality. Proteins are the agents of cellular structure and function and changes observed at the protein level have greater physiological relevance than mRNA abundance changes [7]. Therefore, compared to transcriptomic approaches, proteomics reveals a more direct avenue towards gaining knowledge of what processes renal papillary cells utilize during hyperosmotic stress.

Thus, in the current study we used proteomics to first compare the hyperosmotic renal papilla to an immediately adjacent iso-osmotic region of the kidney, the cortex. Secondly, antidiuresis and diuresis were induced to alter the osmotic environment of the papilla in order to identify osmotically regulated proteins in this region.

Materials and Methods

Mouse treatment and sample collection

Untreated wild-type C57BL/6 mice (Jackson Laboratory, Bar Harbor, ME) (age 6 weeks – 18 months, n=24) were reared under standard laboratory conditions for comparison of cortex and papilla. Antidiuresis was induced in male and female C57 mice (age 1–16 months) via intraperitoneal injection of [deamino-Cys1, D-Arg8] vasopressin (1μg/μl ddAVP in PBS; 1μg ddAVP/g body weight, Sigma V1005) once every 8 hours for 24 hours combined with water deprivation for the same period; a sham group received an injection of PBS alone. Diuresis was induced with addition of sucrose (3%) to drinking water combined with food deprivation. Control mice for this treatment received normal drinking water and food ad libitum. Following treatment mice were euthanized via CO_2 administration. One kidney was dissected to obtain a sample of papilla which was immediately snap-frozen with liquid nitrogen then transferred to −80°C for storage until further processing. A cross-section (2 mm wide) of the other kidney was immersed in 4% paraformaldehyde in PBS and stored at 4°C for up to a week before vacuum infiltration processing and paraffin embedding.

Tissue Processing

Following dissection all tissue samples were manually homogenized on ice using a Dounce homogenizer in RIPA buffer (50 mM Tris-HCl, 140 mM sodium chloride, 1 mM EDTA, 1 mM sodium fluoride, 1 mM sodium (meta)vanadate, 2% CHAPS, 1% NP-40, 1% Triton X-100, 1 tablet mini-tablet Complete protease inhibitor cocktail (Roche, Indianapolis, IN); approximately 5:1 ratio of buffer to sample). Cellular debris was pelleted by centrifugation (19,000g, 4°C, 5 min) and supernatant was stored at −80°C. Protein concentration of each extract was measured using BCA™ Protein Assay Kit (Pierce, Rockford, IL). Absorbances for protein concentration measurements were read using the Spectra FluorPlus plate reader (Tecan, Research Triangle Park, NC) at 560 nm. A portion of the extracted protein was precipitated in acetone (3:1 ratio acetone to sample) overnight at −20°C. Following centrifugation the protein pellet was resuspended in isoelectric focusing (IEF) buffer (7 M urea, 2 M thiourea, 2% CHAPS, 2% NP-40, 15 mM DTE, 0.5% ampholytes pH 3-10NL (Amersham Biosciences, Uppsala, Sweden) 0.002% bromophenol blue).

Once fixed by paraformaldehyde the kidney cross-sections were transferred to vented plastic holding cassettes and immersed in 70% ethanol for 24 hrs then loaded into the Tissue-Tek®VIP® 5 (vacuum infiltration processor; Sakura, Torrance, CA) for processing. Through a graded series of alcohol solutions and organic solvents the samples were ultimately infiltrated by paraffin. The cross-sections were then embedded in paraffin (Tissue-Tek®TEC™ 5; Sakura, Torrance, CA) and cut with a Historange microtome (LKB Bromma #2218-050) at a thickness of 5 μm and mounted on slides with the aid of a heated water bath, after drying at 60°C overnight the slides were stored at room temperature.

Two-dimensional gel electrophoresis

Equal amounts of protein (300 μg) from each replicate in IEF buffer were loaded onto each 11 cm, pH 3-10NL IPG (immobilized pH gradient) strip (Bio-Rad, Hercules, CA) by passive rehydration overnight at room temperature. The sample saturated strips were focused using the IsoelectrIQ (Proteome Systems, Woburn, MA) for at least 60,000 Vhr through a series of voltage increases that reached a maximum of 10,000 V. After completing separation in the first dimension they were stored at −80°C. Proteins were reduced for 5 min and then alkylated for 5 min in equilibration buffer (375 mM Tris-HCl, 6 M Urea, 30% glycerol, 2% SDS) containing 65 mM DTT (dithiothreitol, reduction step) followed by 135 mM iodoacetamide (IAA, alkylation step). Strips were then loaded onto 11% acrylamide/bis slab gels (11.5 cm × 7 cm × 1 mm) and 220 V were applied in an upright SDS-PAGE (Bio-Rad

Criterion Dodeca Cell, Hercules, CA) to separate the proteins based on molecular weight, completing the second dimension. The gels were stained with colloidal coomassie blue (CCB) and densitometry was performed using an Epson 1680 scanner. For the comparison of cortex and papilla each gel was generated from a single animal. Due to the small size of the renal papilla of a mouse samples were pooled with each replicate consisting of tissue from three animals, therefore the four 2D gels prepared for each group represent 12 different animals.

Gel Image Analysis

Scanned images of the gels were analyzed using Delta2D software (Decodon GmbH, Greifswald, Germany) to allow for alignment of the gel images, detection of spots, and quantification of spot volume (see [8]). For the comparison of cortex and papilla the gels were grouped by region with six replicates per group. Alignment of similar spot patterns between gels was accomplished by examining gels as pairs and warping one gel image onto another. The first pair consisted of the first replicate from the cortex group serving as the master gel, whose spot positions do not change, and the second replicate, which was warped to the first. Spot pattern similarity between a gel pair was recognized by the software and automatic match vectors were added to align appropriate regions. All automatic match vectors were manually confirmed and additional match vectors were manually added based on visually determined pattern similarity to refine gel warpings. Next, the third replicate was warped to the second, then the fourth to the third and so on. The first replicate from the papilla group was warped to the first replicate of the control group, then the second to the first and so forth as described above, known as the ‘group warping strategy’. This gel warping strategy was also applied in the hydration state comparison.

Within an experiment all gels were related to all others through the warping strategy; therefore, regions could be appropriately aligned between all gels. A fusion of all the gels within an experiment produced a cumulative proteome map of all proteins present. The comprehensive maps were used for spot detection. Background and intensity thresholds were altered on display without affecting the intensity data to optimize the spot outlines generated by the software, followed by manual refinement of spot outlines to maximize accuracy of subsequent quantitation. Spot outlines were then exported to all gel images and normalization proteins were selected based on high expression (top 20%) without significant variation between groups. All spots were assigned a numerical value based on the stain intensity within the spot boundary as a function of the sum of the stain intensities of the normalization proteins providing an internal control that is consistent between groups. The ratios between spot volumes on regional and hydrations state gels and their appropriate controls along with t-Test values for the significance of the difference were generated using the Delta 2D software; these data were used to identify protein spots of interest.

Spot Processing

The following procedures were conducted, when possible, in a flow hood equipped with a hepafilter to minimize particulate contamination (Hazard Technology, Millersville, MD) using MilliQ water (Millipore, Billerica, MA). Spots of interest were excised from gels using a tissue array punch (1.5mm diameter) and stored at −80°C until further processing. For the comparison of papilla and cortex peptide extraction was performed using the Montage In-Gel Digest$_{ZP}$ Kit (Millipore, Billerica, MA) which contains a 96-well plate C18 resin to bind peptides fixed within the base of the well. Each gel spot was placed into a separate well and destained once (100 μl/well, 30 min) with 25 mM ammonium bicarbonate/ 5% acetonitrile and twice (100 μl/well, 30 min each) with 25 mM ammonium bicarbonate/ 50% acetonitrile. Acetonitrile was added to dehydrate the spots. It was then removed and the spot was rehydrated with stabilized trypsin (Promega, Madison, WI Cat. No. V5280 (166

ng/well) in 25 mM ammonium bicarbonate (10 μl/well). The plate was incubated overnight at 37°C in a sealed bag to prevent evaporation. The resin was wet with a small amount of acetonitrile to allow pepides to bind and peptides were extracted from the spots twice with 0.2% trifluoroacetic acid (TFA) (first with 130 μl/well, second with 100 μl/well, 30 min each). Peptides bound to the resin were then eluted with 2.5 μl 0.1%TFA/50% acetonitrile. Eluent was spotted onto a solid MALDI target (Applied Biosystems, Foster City, CA) and overlaid with 0.5 μl matrix (α-cyano-4-hydroxycinnamic acid) (10 mg/ml in 60% acetonitrile/0.1% TFA/10 mM ammonium phosphate).

For the hydration state comparison spots stain was removed with multiple washes of 100 mM ammonium bicarbonate/50% acetonitrile for 2–3 hrs. The spot was then dehydrated with acetonitrile and rehydrated with a 50mM ammonium bicarbonate solution containing trypsin (5μg/μl, 5 μl per spot) for 30 min at 4°C, then transferred to 37°C and incubation overnight. Peptides were then extracted twice with 10 μl 60% acetonitrile/1% trifluoroacetic acid (TFA) 2–3 hrs. Pooled extracts were dried to <1 μl (ISS 110 SpeedVac, Waltham, MA) and resuspended in 9 μl 0.5 % TFA. ZipTips® (Millipore) were then used to clean and concentrate the peptide extracts. ZipTips® contain a resin that binds the peptides allowing them to be separated from salts and other contaminants that remain in solution. The resin is wet with acetonitrile to allow the peptides to bind then equilibrated with a 0.1% TFA solution. The sample was loaded onto the resin within the ZipTip® by repeated pipetting followed by a wash with 0.1% TFA. Peptides were then eluted into 1.5 μl of 60% acetonitrile/0.1% TFA. Eluent was spotted onto a solid MALDI target and overlaid with 0.5 μl matrix (α-cyano-4-hydroxycinnamic acid) (10 mg/ml in 60% acetonitrile/0.1% TFA/10 mM ammonium phosphate).

Mass Spectrometry

Matrix assisted laser desorption ionization (MALDI) was the chosen technique for this analysis. The mass spectrometer, a 4700 Proteomics Analyzer (Applied Biosystems, Foster City, CA), was used to make time-of-flight (TOF) measurements of peptides ionized by a laser and the intensity of each peptide peak was also recorded creating a mass spectrum.

This analysis used two methods to achieve peptide fragmentation. First, post-source decay (PSD) utilized the spontaneous fragmentation that occurs following laser ionization of peptides. Second, following ionization by the laser, the accelerated peptides are introduced into a collision cell where they collide with gas molecules causing fragmentation in a process called collision induced dissociation (CID) [9].

Each set of spectra was searched against the SwissProt database using Mascot (Matrix Science) -interfaced with GPS Explorer (Applied Biosystems, Foster City, CA) software. The resulting identifications were assigned scores based on the probability that the match was non-random with high scores indicating a higher probability that the identification is not due to chance. Scores above 67 are significant at the level of $p<0.05$. For the purposes of this analysis identifications with scores ≥90 and molecular weight and isoelectric point values that agreed with the position on the gel were considered valid.

Western Blot

Tissue extract in RIPA buffer was reserved from all dissected samples to conduct a western blot. Equal volumes of sample and 2x Laemmli buffer (125 mM Tris HCl, 4% SDS, 20% glycerol, 0.004% bromophenol blue and 10% β-mercaptoethanol added fresh) were combined and boiled for 5 min in sealed tubes. They were then loaded onto a SDS-PAGE (Mini-Protean II Bio-Rad, Hercules, CA) gel and 120 V were applied for approximately 75 min to allow proteins to migrate in the gel. Equal amounts of protein were loaded onto each

lane as determined by the BCA™ Protein Assay Kit (Pierce, Rockford, IL). The gel was then sandwiched against a piece of PVDF membrane, between soaked blotting papers in transfer buffer (48 mM Tris, 39 mM glycine, 0.04% SDS, 20% methanol), and transferred for 90 min (Trans-Blot SD Semi-Dry Transfer Cell Bio-Rad, Hercules, CA). The membrane was then blocked with 3% non-fat milk in tris-buffered saline (TBS) and incubated with either anti-α B-crystallin (rabbit polyclonal SPA-223, Stressgen, Ann Arbor, MI; 1:5,000) or anti-lactate dehydrogenase (rabbit polyclonal ab53010, Abcam, Cambridge, MA; 1:1,000) primary antibody in TBS with 2% non-fat milk overnight at 4°C or 2 hr at room temperature. For the hydration state comparison two primary antibodies were used: anti-Hsp25 (rabbit polyclonal SPA-801, Stressgen, Ann Arbor, MI; 1:1000), and anti-Hsp70 (rabbit polyclonal SPS-812C, Stressgen, Ann Arbor, MI; 1:1000). After several washes with 0.05% Tween-20 in TBS the membrane was incubated with horseradish peroxidase conjugated secondary antibody (donkey anti-rabbit Fab_2 fragment 711-036-152, Jackson Immunoresearch West Grove, PA; 1:50,000) in TBS with 2% non-fat milk for 1 hr at room temp. The membrane was washed with 0.05% Tween-20 in TBS several times and rinsed with MilliQ then covered with chemiluminescent detection solution that reacts with HRP (Supersignal West Femto Maximum Sensitivity Substrate Kit, Pierce, Rockford, IL). Images of the western blot were collected and imported into ImageQuant software for densitometry analysis. Following the transfer the acrylamide gel was stained with CCB to confirm equal protein loading.

Immunohistochemistry

Slides prepared from paraffin embedded kidney cross-sections were deparaffinized with xylenol followed by washes in a graded series of decreasing ethanol solutions and finally TBS. Antigen retrieval was performed by immersion in boiling citrate buffer (10mM sodium citrate, pH 6.0) for 15 min. Slides were then blocked with 2% bovine serum albumin (BSA) in PBS for 1hr at room temperature. The slides were incubated in either anti-α B-crystallin (rabbit polyclonal SPA-223, Stressgen, Ann Arbor, MI; 1:500) or anti-lactate dehydrogenase (rabbit polyclonal ab53010, Abcam, Cambridge, MA; 1:50) primary antibody in PBS with 2% BSA for 2 hr at room temperature. After three washes with PBS the slides were incubated with horseradish peroxidase conjugated secondary antibody (donkey anti-rabbit Fab_2 fragment 711-036-152, Jackson Immupnoresearch, West Grove, PA; 1:10,000). Detection of the HRP conjugated to the secondary antibody was performed using diaminobenzibine (DAB) (ImmPACT DAB, Vector Laboratories, Burlingame, CA) which is converted to a brown product in the presence of HRP. Detection was also performed on slides incubated with each antibody alone to control for endogenous HRP activity. Images were collected using a Wild Heerbrugg type 181300 (Switzerland) dissecting microscope.

Pathway Analysis

The PANTHER website (Protein Analysis Through Evolutionary Relationships pantherdb.org) assisted in the classification of proteins according to molecular function(s) and biological process(es) with which they are involved or related. The lists of identifications from cortex and papilla were separately compared to the total list of mouse genes (NCBI: *Mus musculus*) for significant over- or under-representation of molecular functions or biological processes. For the comparison of hydration states lists of identified proteins related to each condition were created and individually compared to the total list of mouse genes (NCBI: *Mus musculus*) for significant over- or under-representation of molecular functions or biological processes (i.e., up-regulated during antidiuresis, down-regulated during antidiuresis, up- or down-regulated during antidiuresis, up-regulated during antidiuresis or down-regulated during diuresis, etc.). Statistical analysis for the significance of the results were determined by comparing the fraction of genes involved with a particular function or process from a regional or hydration state list with the fraction of genes involved

with that function or process in the total mouse genome. Additionally, because the number of functions and processes tested is so large a Bonferroni correction is made to be conservative since repeated testing increases the chances of false positives.

Results

Identification of proteins characteristic of renal papilla and cortex in untreated mice

The proteome map prepared from the outermost part of the mouse kidney, the cortex, was compared to that of the innermost region, the renal papilla using Delta 2D software (fig. 1). Fusion of the two maps led to a total of 1877 proteins present in either region. The overlay image (fig. 1C) provides a visual representation of the expression comparison made between identical gel regions. Spot outlines provide boundaries for the expression quantification of an individual spot. Spot intensities were compared (t-Test, $p<0.05$) to determine which proteins were regulated, defined here as greater than 2-fold expression difference within a region relative to the other. The cortex contained 212 proteins, labeled C01 – C212, significantly over-expressed relative to papilla while the papilla had 80 proteins, P01 – P80, with significantly increased expression relative to the cortex.

Analysis of the proteins over-expressed in the papilla led to the identification of 22 proteins which contained 16 different proteins (Table 1). Analysis of the proteins over-expressed in cortex led to the identification of 51 different proteins (Table 2) representing a total of 38 different proteins. Several of these proteins contain redundant identifications representing posttranslational variants of a single protein. The majority of protein identifications (63%) had MASCOT (Matrixscience, Inc.) scores above 200 and a false discovery probability on the order of 10^{-20}.

Figure S1 provides a representation of how each spot was analyzed using mass spectrometry. An MS spectrum and several MS/MS spectra were collected for each spot and used in a MASCOT search using the SwissProt database for identifications.

Identification of proteins altered during diuresis and antidiuresis in mouse renal papilla

Efficacy of the treatment performed to alter the osmolality within the kidney was confirmed via urine osmolality measurement. At the start of treatment the average urine concentration of all groups combined was 1978 mOsm (± 166). After 24 hrs mice that were deprived of water and administered vasopressin produced urine with increased osmolality of 3000 mOsm (± 325) In contrast, mice deprived of food but given sucrose (3%) water produced a very dilute urine of 243 mOsm (± 152).

Proteome maps prepared from the papillae of antidiuretic and diuretic mice were compared to maps from sham injected and control mice, respectively. A total of 519 spot outlines on a fusion map of all conditions were used for quantification to determine spot differences due to osmolality treatment. Average spot volume intensities (n=4) were compared between each treatment group and its control group to generate a ratio equal to the fold change and a p-value of a t-Test for significant difference between the groups. Proteins with greater than 1.25-fold change in expression and t-test p-values below 0.1 were selected for further examination (fig. 2). The initial selection of these proteins was made based on the statistical tool provided by the Delta2D software termed ‘Pavlividis Template Matching’, which allows the selection of an expression profile and matches proteins accordingly at a p-value threshold. A total of 110 proteins satisfied this condition: 40 proteins were up-regulated during antidiuresis, 20 proteins were down-regulated during antidiuresis; 30 proteins were up-regulated during diuresis, 20 proteins were down-regulated during diuresis. There are 13 incidents of redundancy such that 110 labels for proteins changing under either antidiuresis or diureisis conditions correspond to 97 different outlines. Figure 3 provides a representation

of the quantification performed to determine up- and down-regulation during antidiuresis or diuresis. Spot expression data are also displayed using a heat map to color-code expression of a spot and provide a side-by-side comparison of replicates between treatment and control groups (fig. 4).

The identified proteins for proteins differentially expressed in the renal papilla following treatment to alter osmolality are listed in Tables 3 and 4. In addition to the MASCOT score the number of peptides from the MS spectrum that were used for identification is listed with the percentage of sequence coverage. The theoretical isoelectric point and molecular weights are provided as well as the fold change determined by Delta 2D analysis of the proteome maps. Overall, 18 different proteins were identified representing 15 different proteins that change during antidiuresis (Table 3). Eleven of the spots (and proteins) were up-regulated while 7 spots, representing 5 proteins, were down-regulated. A single identification was found to reoccur in both up- and a down-regulated proteins (spots P36, P49, P53) suggesting posttranslational modification.

Analysis of the proteins differentially expressed during diuresis produced 18 different protein identifications in 21 spots due to three proteins producing the same identification (proteins P107, P108, P109) (Table 4). Twelve proteins (in 13 proteins) were up-regulated while 6 proteins (in 8 spots) were down-regulated.

Confirmation of protein expression differences using Western blots and immunohistochemistry

Three proteins (P10, P12, and P13) over-represented in the renal papilla were identified as αB crystallin; these proteins were highly over-represented with P13 expression >17-fold relative to cortex. To substantiate the findings made during the proteomic analysis a subsequent western blot was performed using an antibody against αB crystallin. Tissue homogenate from papilla produced a distinct band while no band is seen for cortex (fig. 5A). Likewise, when an antibody against lactate dehydrogenase (P70, P75, and P84) was used a band was produced in cortex but not in papilla (fig. 5A). Quantification of band volume was performed for six replicates of each tissue type and antibody (fig. 5B, C) and significant p-values are reported (fig. 5D).

Figure 6 displays the regional over-representation of αB crystallin in the papilla (fig. 6A) and lactate dehydrogenase in the cortex (fig. 6B) observed in a mouse kidney cross-section via immunohistochemistry. Brown stain concentrated within the tip of the renal papilla (fig. 6A) indicates the presence of αB crystallin protein. The papilla is unstained in figure 6B while the Cortex and outer medulla are stained with brown reaction product indicating the presence of lactate dehydrogenase protein.

Hsp70 (spot 4) was identified as being up-regulated during antidiuresis while expression of Hsp beta-1 (spotss P41 and P43) was down-regulated under this condition according to spot intensities measured from the 2D gels. A western blot performed on tissue homogenates (n=6) from antidiuretic and sham injected mice using antibodies against Hsp70 and Hsp25 (also known as Hsp beta-1) provided significant support for up-regulation of Hsp70 with antidiuresis (fig. 7). While the trend of decreased expression of Hsp25 during antidiuresis is supported by the western blot the variability between replicates prevents the difference from being statistically significant (fig. 7B, C and D). This result was unexpected and may be due to different isoforms or variants of small heat shock protein HSP25/HSP beta-1 being recognized by the antibody relative to the spots detected on 2D gels.

Functional significance of proteins characteristic of renal papilla versus cortex

Identifications from each kidney region were grouped according to the biological processes and molecular functions with which they are involved using the PANTHER software. Chaperone functioning, particularly the Hsp90 family, is significantly over-represented in the papilla (Table 5); associated with this the processes of protein folding and the stress response are significantly over-represented. This is due to the identification of Hsp beta-1 (P18), Hsp90 (P60), 14-3-3 (P24) and endoplasmin (P70) in this region. Other processes that are abundantly represented but not significantly over-represented in the renal papilla are transport (serotransferrin (P57), albumin (P51), actin (P45) and transitional ER ATPase (P67)), intracellular protein trafficking (actin (P45), transitional ER ATPase (P67), ADP-ribosylation factor (P03) and calmodulin (P07)), signal transduction (Rho GDP-dissociation inhibitor (P16), calmodulin, and 14-3-3 (P24)) and muscle contraction (tropomyosin 3 (P25) and αB crystallin (P10, P12, P13). Additionally, αB crystallin has structural functions and is involved in visual perception, glutathione S-transferase (P17, P22, P23) is associated with detoxification, and aldose reductase (P26, P28, P29, P32) is a metabolic enzyme with oxidoreductase activity and involved in osmolyte synthesis.

The general theme of the cortex is an increase in expression of proteins associated with metabolism when compared to the papilla. Specifically, carbohydrate metabolism was the dominant process over-represented with 16 protein identifications involved (Table 5). The most common function of these proteins was oxidoreductase/dehydrogenase activity represented by malate dehydrogenase (C62), isocitrate dehydrogenase (C126), 2-oxoglutarate dehydrogenase (C135), L-lactate dehydrogenase (C70, C75, C84), hydroxyacid oxidase 3 (C79), alcohol dehydrogenase (C77), quinone oxidoreductase (C80), sorbitol dehydrogenase (C91, 95), and enoyl-CoA hydratase (C25, C26, C55), which is also a lyase. Lyase activity is represented by aconitate hydratase (C190, C191, C192), carbonic anhydrase (C31), enolase (C130, C138), and fructose bisphosphate aldolase (C82). Carbohydrate metabolism is further represented in the cortex by fructose bisphosphatase (C69), pyruvate carboxylase (C210), ketohexokinase (C42), and succinyl-CoA:3-ketoacid-CoA transferase 1 (C162).

The process of amino acid metabolism was prevalent with several related functions represented as follows: methylmalonate-semialdehyde dehydrogenase (C153, C156, C157), glutamate dehydrogenase (C158, C154) and Δ-1-pyroline-5-carboxylate dehydrogenase (C180) for oxidoreductase activity; ornithine aminotransferase (C122) and gycine amidinotransferase (C129) for transferase activity; glutamine synthetase (C127) and argininosuccinate synthase (C117) function as ligases; lastly, aspartoacylase 2 (C62) has hydrolase activity. Additional protein metabolism enzymes identified were acetyl-CoA acetyltransferase (C93, C99) and protein disulfide isomerase (C164, C170).

Proteins associated with fatty acid metabolism are also abundant in the cortex. These include succinyl-CoA:3 ketoacid-CaA transferase 1 and enoyl-CoA hydratase (C162) already mentioned above, which have roles in both carbohydrate and fat metabolism. Acyl-CoA dehydrogenase (C105, C107, C108) participates in fatty acid metabolism and electron transport, a process also represented by dihydrolipoyl dehydrogenase (C175) and electron transfer flavoprotein (C22). Oxidoreductase functioning outside basic metabolic processes was represented by peroxiredoxin 5 (C20), categorized as being involved in antioxidation and free radical removal. The remaining identifications are less easily grouped with the others; calbindin (C12) is involved in signal transduction, NDRG-1 (C119) is involved in cell proliferation and differentiation, and ATP synthase is unclassified for function or process by PANTHER.

Functional significance of renal papillary proteins altered during diuresis and antidiuresis

The identified proteins listed in Table 3 and 4 were compared to the whole mouse proteome using the PANTHER software to determine if particular biological processes or molecular functions were altered by osmolality changes in the renal papilla. The list of identifications up-regulated by antidiuresis was combined with the identified proteins down-regulated by diuresis to generate a list of proteins whose increased expression is associated with increased urine osmolality (Table 6). Proteins associated with immunity and defense processes that are significantly overrepresented in this list include peroxiredoxin 2 and 6, Hsp70 (spot P4), Hsp beta-1 (proteins P41 and P43), abhydrolase domain-containing protein 14B (spots P9 and P105), fibrinogen (spot P101), and translationally-controlled tumor protein (spot P96). Antioxidant and free radical removal processing and peroxidase functioning was also over-represented in this list (peroxiredoxin 2 and 6, proteins P37 and P22). Additionally, glycolysis was an over-represented process due to the papillary regulation of α-enolase (spot P36) and L-lactate dehydrogenase (spot 40). Interestingly, α-enolase was also identified in two spots down-regulated during antidiuresis (spots P49 and P53). The presence of α-enolase in multiple positions within the gels implies post-translational modification as a mechanism for alteration of this protein.

Proteins that change during antidiuresis reveal significant up-regulation of chaperone functioning when compared against the whole mouse proteome. These proteins include T-complex protein 1 (spot P47), Hsp beta-1 and Hsp70 (Table 6). These three proteins are also associated with the process of protein folding, which is is also significantly affected by antidiuresis in the papilla. This list also reveals a significant over-representation of oxidoreductase functioning associated with the identification of L-lactate dehydrogenase, peroxiredoxin 2 and 6, acyl-CoA dehydrogenase (spot P60) and aldose reductase (spot P63). While not statistically significant (p=0.0564) the list of identifications that change during diuresis contains four proteins that are related to the cytoskeleton: actin (spot 69), tubulin (spots P62 and P88), α-actininin 4 (spots P76 and P17) and translationally-controlled tumor protein (spot P96). Two of these identifications, actin (spots P69 and P19) and α-actininin 4 (spots P17 and P76) are also up-regulated during antidiuresis. Similarly, peroxiredoxin 2 (spots P37 and P82) is up-regulated during both antidiuresis and diuresis. In contrast, abhydrolase domain-containing protein 14B is up-regulated during antidiuresis (spot P9) and down-regulated during diuresis (spot P105).

Cadherin-16 (spot 3, cell adhesion-mediated signaling), EH domain-containing protein (spot P5, membrane trafficking), and glyceraldehyde-3-phosphate dehydrogenase (spot P38)are all up-regulated during antidiuresis but not associated with an over-represented function or process. Guanine nucleotide-binding protein (spot P55) is down-regulated during antidiuresis and associated with signal transduction but this process is not over-represented.

Aside from the cytoskeletal proteins mentioned earlier the proteins up-regulated during diuresis are not easily grouped into a common process or function. These proteins include acidic leucine-rich nuclear phosphoprotein (spot P75), Rho GDP-dissociation inhibitor 1 (spot P77), antithrombin-III (spot P61), are all spectrin (spot P64), α B-crystallin, dihydropyrimidinase-related protein 2 (spot P74), ffumarate hydratase (spot P79), major urinary protein 2 (spot P93), serotransferrin (spots P107, P108, and P109), and40S ribosomal protein (spot P104).

Discussion

The complexity of the renal cortex proteome is higher than that of the renal papilla

The fusion of proteome maps from renal cortex and papilla produced 1877 proteins, indicating substantial functional complexity within the tissue while also offering support for

the resolving power of two-dimensional gels [10]. Examining the proteins whose expression difference was greater than 2-fold ($p<0.05$) between regions revealed more than twice as many (212) proteins over-represented in the cortex compared to the papilla (80). This seems likely due in part to the overall greater complexity observed in the proteome map of cortex compared with papilla (fig. 1A and B). The greater cell type heterogeneity of the cortex could explain the higher complexity observed at the proteome level. The papilla is composed of fewer tissue and cell types reflected by a lesser complexity of its proteome.

Stress response and cytoskeletal stabilizer proteins characterize the renal papilla

A significant portion of the identified proteins that are over-represented in the papilla have chaperone function associated with protein folding (Table 5). Heat shock proteins (HSPs) are an abundant, highly conserved group of molecular chaperones. The observed over-representation of Hsp90, Endoplasmin (GRP94), and transitional endoplasmic reticulum (TER) ATPase in the papilla suggests a greater prominence of the protein folding machinery [11], regulation of mineralocorticoid receptor and aldosterone signaling [12], and/or regulation of the transcription factor TonEBP [13]. Together the identification of TER ATPase and ARF1 suggests that Golgi apparatus functioning contributes to the osmotolerant phenotype, potentially through trafficking and removal of damaged proteins [14]. Removal of protein damage as an important process in the papilla is further substantiated by the over-representation of two isoforms (mu1 and mu2) of glutathione S-transferase (GST). Another protein over-represented in the papilla, which has also been associated with aldosterone mediated sodium reabsorption in the collecting duct is 14-3-3 epsilon. 14-3-3 epsilon stabilizes apical sodium channels in the epithelium of the collecting duct by preventing them from being degraded [15]. In neurons 14-3-3 has also been observed to interact with a signaling complex responsible for cytoskeletal rearrangement [16].

Along with chaperone and cytoskeletal stabilizing functions two small HSPs were identified as over-represented in the renal papilla in our study: Hsp beta-1 (also known as murine Hsp25 and human Hsp27) and αB crystallin (23 kDa). These data support the view that hypertonicity causes functional interaction of small molecular chaperones and cytoskleletal proteins leading to structural stabilization [17–19]. In rats expression of αB crystallin has also been observed to follow the corticopapillary osmotic gradient with higher expression in areas of increased hypertonicity and to increase in hypertonically stressed cultured cells [20]. Further support for cytoskeletal stabilizing processes being major targets for counteracting cytoskeletal strain during hypertonic stress comes from studies in which increased osmotic pressure altered the interaction between tropomyosin and actin [21], changed tropmyosin isform expression [22], and increased medullary expression of tropomyosin following vasopressin treatment [23].

Osmotic stress increases the level of actin in a variety of cells [24,25]. In renal epithelium the mechanism for the increase in actin is related to the inhibition of cofilin, which cleaves actin chains [26]. Inhibition of cofilin also transiently inhibits apoptosis and is, at least in part, a result of phosphorylation by Rho [26]. Through its effect on actin, Rho inhibits the insertion of aquaporin 2 (AQP2) in the apical membrane of collecting duct cells [27]. Furthermore, over-representation of Rho GDP-dissociation inhibitor 2 in the papilla supports the potential importance of this signaling pathway in the papilla. GDP-dissociation inhibitors (GDIs) inactivate Rho since, as a GTPase, it must bind and hydrolyze GTP to remain active. When binding to GDP is prolonged the protein is inactive, thus, the inhibition of cofilin by Rho would be prevented by an active GDI [28]. Rho involvement in AQP2 insertion and actin rearrangement, while also contributing to the inhibition of apoptosis [27,29] illustrates the elegance of the adaptation of these cells to their environment since signaling that corrects a problem simultaneously allows time for the correction. Besides Rho-mediated signaling, over-representation of calmodulin in the papilla suggests that

calcium-regulated signaling also targets the cytoskeleton by promoting formation of actin stress fibers [30]. In addition, calmodulin regulates taurine transporters that are responsible for the uptake of taurine, a compatible osmolyte [31]. Another protein that is over-represented in the papilla and contributes to organic osmolyte accumulation is aldose reductase [32–34]. In our analysis aldose reductase was identified in four proteins over-represented in papilla. Three proteins varied predominantly in isoelectric point while the forth represented a shift in molecular weight (see fig 2.1C, P26, P28, P29, and P32). The presence of a protein in multiple proteins suggests potential PTMs. The addition/removal of a phosphate group, which is highly negatively charged but has a small delta mass is a PTM in agreement with the observed data.

Proteins functioning in oxidative metabolism are increased in renal cortex compared to papilla

The vast majority of identified proteins over-represented in the renal cortex, when compared to the papilla, are associated with oxidative metabolism (Table 3). The significantly over-represented functions of dehydrogenation and oxidoreduction refer to the electron transfer associated with many metabolic enzymes. The process of carbohydrate metabolism was most prominent but a wide array of other processes were also over-represented, including amino acid metabolism, the citric acid cycle, fatty acid metabolism and electron transport. Energy demands in the cortex are high due to the presence of the proximal tubule which is responsible for the majority of reabsorptive active transport. Over-representation of enzymes associated with aerobic metabolism, including those that participate in the citric acid cycle (aconitate hydratase, malate dehydrogenase and isocitrate dehydrogenase), are further expected in the cortex given the increased availability of oxygen in the cortex due to increased blood flow when compared with the papilla.

Stabilization of cell integrity by papillary proteins that are up-regulated during antidiuresis

Several proteins identified as up-regulated during antidiuresis support our observation that hyperosmolality in the renal papilla requires stabilization of the cytoskeleton and protein folding (see above). These include cadherin-16, α-actinin-4, EH domain-containing protein 4 (EHD4), GAPDH, actin, and HSP70. Cadherin-16 is specifically expressed in the kidney and, unlike most other members of the cadherin family, it cannot bind catenin. Therefore it does not participate in the adherens junction, a classic cell-cell connection. Rather, cadherin-16 has been observed to interact with αB crystallin and to colocalize with actin (which we also found to be up-regulated during antidiuresis) in the renal collecting duct [35]. In the renal papilla actin and α-actinin-4 were found to be associated with a protein complex thought to be involved in AQP2 trafficking [36]. These water channels are trafficked to, and inserted in, the membrane during antidiuresis to facilitate the generation of concentrated urine via water reabsorption from the ultrafiltrate. Thus, the up-regulation of α-actinin-4 promotes water reabsorption in the CD. Trafficking of AQP2 could be promoted by EHD4 as this protein has been implicated in the trafficking of early endosomes [37,38] and endocytosis regulates the distribution of AQP2 and the epithelial sodium channel (ENaC), both of which are critical for urine concentration [39].

Additional proteins that are up-regulated during antidiuresis include abhydrolase domain-containing protein 14B, which is a transcription factor known as CCG1 (cell cycle arrest in G_1)-interacting factor B (CIB), α-enolase, glyceraldehyde-3-phosphate dehydrogenase (GAPDH), lactate dehydrogenase (LDH), and peroxiredoxins 2 and 6. Both peroxiredoxins and GAPDH are antioxidant proteins involved in cell protection against oxidative damage [40–42]. Importantly, the generation of ROS may lead to more than just oxidative damage as GAPDH and peroxiredoxins have been implicated in cell signaling following hyperosmotic stress [43]. Following oxidative stress in a variety of cell types GAPDH increases in

expression and translocates to the nucleus leading to apoptosis [44]. Furthermore, in the nucleus GAPDH and LDH (which is also up-regulated during antidiuresis) participate in the OCA-S (octamer-binding factor 1 co-activator in S-phase) transcription co-activator complex [45]. The OCA-S links the NAD^+/NADH redox state to cell cycle progression by utilizing GAPDH as a redox sensor and the enzymatic activity of LDH to reduce histone (H2B) expression when NAD^+ levels are low, as would occur following DNA damage, thereby leading to activation of the cell-cycle checkpoint [45]. In culture, stressed cells showed colocalization of GAPDH and stress fibers [46] and GAPDH is also involved in endocytosis and DNA repair in a manner that appears to be dependent on cellular localization [47].

Proteins that are up-regulated during diuresis confer structural stability

Many identifications of proteins up-regulated during diuresis follow the theme of alteration to cell structural components. Two proteins were identified as tubulin, the globular protein that makes up microtubules and represents an essential component of the cytoskeleton involved in both cell structure and vesicular transport. Alterations in tubulin support the need for up-regulation of αB crystallin as a molecular chaperone to prevent aggregation, as has been observed in the lens [48]. In addition to two tubulin variants dihydropyrimidinase-related protein 2 is up-regulated during diuresis and because this protein has been linked to microtubule reorganization in axons [49] it further supports the notion that microtubule dynamics is altered during diuresis. The up-regulation of αB crystallin and actin during both diuresis and antidiuresis supports the reorganization of the cytoskeleton necessary following both swelling and shrinking that occur with osmotic stress. Likewise, antidiuresis and diuresis both affect AQP2 trafficking and insertion into the plasma membrane. A role of α-actinin-4 in these processes has been observed [36], and is supported in this analysis by up-regulation of this protein during diuresis and antidiuresis. Another up-regulated protein during diuresis, spectrin, was identified as a component in what Noda et al. [36] termed the ‘force generator complex’ involved in the trafficking of AQP2. Spectrin associates with the Golgi apparatus as part of the membrane cytoskeleton [50] and its up-regulation could affect AQP2 trafficking during diuresisdieresis in addition to stabilizing the cytoskeleton. Examination of the cytoskeleton in brain cells showed colocalization of actin, tubulin, spectrin, GAPDH and dihydropyrimidinase-related protein 2 [51]. Since all these proteins (with the exception of GAPDH) are major cytoskeletal components and up-regulated during diuresis it is likely they stabilize the cytoskeleton via complex formation.

Summary and Conclusions

We have shown that renal cortical and papillary proteomes differ significantly and that proteome complexity is greater in the cortex, which corresponds well with greater tissue and cell type heterogeneity. Many proteins over-represented in the paplla compared to cortex have chaperone functions associated with protein folding and/or cytoskeleton dynamics. In contrast, proteins over-represented in cortex are characteristic of oxidative metabolism, which is in agreement with greater metabolic activity and blood supply in cortex. The proteome of the papilla is plastic and altered significantly in response to tonicity changes. In addition to cytoskeletal proteins, metabolic enzymes and molecular chaperones were were associated with extracellular osmolality as well as proteins involved in redox balance, transport and transcription. A common theme throughout our analysis of osmotic effects on the renal proteome has been the identification of proteins that function in multiple processes but share a common involvement in the regulation of cytoskeleton and protein stability as well as protein folding and trafficking.

Supplementary Material

Refer to Web version on PubMed Central for supplementary material.

References

1. Ditrich, H. Renal structure and function in vertebrates. Science Publishers; Enfield(NH), USA: 2005.
2. Garcia-Perez A, Burg MB. Renal medullary organic osmolytes. Physiol Rev 1991;71:1081–1115. [PubMed: 1924548]
3. Jespersen B. Regulation of renal sodium and water excretion in the nephrotic syndrome and cirrhosis of the liver, Dan Med Bull. 1997;44:191–207.
4. Yancey PH, Clark ME, Hand SC, Bowlus RD, Somero GN. Living with water stress: evolution of osmolyte systems. Science 1982;217:1214–1222. [PubMed: 7112124]
5. Garcia-Perez A, Burg MB. Importance of organic osmolytes for osmoregulation by renal medullary cells. Hypertension 1990;16:595–602. [PubMed: 2246026]
6. Neuhofer W, Beck FX. Cell survival in the hostile environment of the renal medulla. Annu Rev Physiol 2005;67:531–555. [PubMed: 15709969]
7. Theodorescu D, Mischak H. Mass spectrometry based proteomics in urine biomarker discovery. World J Urol 2007;25:435–443. [PubMed: 17703310]
8. Valkova N, Kultz D. Constitutive and inducible stress proteins dominate the proteome of the murine inner medullary collecting duct-3 (mIMCD3) cell line. Biochimica Et Biophysica Acta-Proteins and Proteomics 2006;1764:1007–1020.
9. Lopez-Ferrer D, Canas B, Vazquez J, Lodeiro C, Rial-Otero R, Moura I, Capelo JL. Sample treatment for protein identification by mass spectrometry-based techniques. Trac-Trends in Analytical Chemistry 2006;25:996–1005.
10. Gorg A, Weiss W, Dunn MJ. Current two dimensional electrophoresis technology for proteomics (vol 4, pg 3665, 2004). Proteomics 2005;5:826–827.
11. Frydman J, Hohfeld J. Chaperones get in touch: The hip-hop connection. Trends in Biochemical Sciences 1997;22:87–92. [PubMed: 9066258]
12. Nemoto T, Oharanemoto Y, Sato N, Ota M. Dual roles of 90-kDa heat-shock protein in the function of the mineral corticoid receptor. Journal of Biochemistry 1993;113:769–775. [PubMed: 8396573]
13. Chen Y, Schnetz MP, Irarrazabal CE, Shen RF, Williams CK, Burg MB, Ferraris JD. Proteomic identification of proteins associated with the osmoregulatory transcription factor TonEBP/OREBP: functional effects of Hsp90 and PARP-1. American Journal of Physiology-Renal Physiology 2007;292:F981–F992. [PubMed: 17148781]
14. Bui QT, Golinelli-Cohen MP, Jackson CL. Large Arf1 guanine nucleotide exchange factors: evolution, domain structure, and roles in membrane trafficking and human disease. Mol Genet Genomics 2009;282:329–350. [PubMed: 19669794]
15. Liang XB, Butterworth MB, Peters KW, Walker WH, Frizzell RA. An obligatory heterodimer of 14–3-3 beta and 14–3-3 epsilon is required for aldosterone regulation of the epithelial sodium channel. Journal of Biological Chemistry 2008;283:27418–27425. [PubMed: 18687683]
16. Angrand PO, Segura I, Volkel P, Ghidelli S, Terry R, Brajenovic M, Vintersten K, Klein R, Superti-Furga G, Drewes G, Kuster B, Bouwmeester T, Acker-Palmer A. Transgenic mouse proteomics identifies new 14–3-3-associated proteins involved in cytoskeletal rearrangements and cell signaling. Molecular & Cellular Proteomics 2006;5:2211–2227. [PubMed: 16959763]
17. Neuhofer W, Muller E, Burger-Kentischer A, Beck FX. Hypertonicity affects heat shock protein 27 and F-actin localization in Madin-Darby canine kidney cells. Kidney International 1998;54:S165–S167. [PubMed: 9736278]
18. Djabali K, de Nechaud B, Landon F, Portier MM. AlphaB-crystallin interacts with intermediate filaments in response to stress. J Cell Sci 1997;110(Pt 21):2759–2769. [PubMed: 9427392]
19. Arai H, Atomi Y. Chaperone activity of alpha B-crystallin suppresses tubulin aggregation through complex formation. Cell Struct Funct 1997;22:539–544. [PubMed: 9431459]

20. Michl M, Ouyang N, Fraek ML, Beck FX, Neuhofer W. Expression and regulation of alpha B-crystallin in the kidney in vivo and in vitro. Pflugers Archiv-European Journal of Physiology 2006;452:387–395. [PubMed: 16680485]
21. Schwienbacher C, Magri E, Trombetta G, Grazi E. Osmotic properties of the calcium-regulated actin filament. Biochemistry 1995;34:1090–1095. [PubMed: 7827025]
22. Dihazi H, Asif AR, Agarwal NK, Doncheva Y, Muller GA. Proteomic analysis of cellular response to osmotic stress in thick ascending limb of Henle's loop (TALH) cells. Molecular & Cellular Proteomics 2005;4:1445–1458. [PubMed: 15975915]
23. Khegay II, Katokhin AV. Expression of tropomyosin-encoding gene in the kidney depends on functioning of vasopressin gene. Biochemical Genetics 2004;42:61–67. [PubMed: 15068339]
24. Pedersen SF, Mills JW, Hoffmann EK. Role of the F-actin cytoskeleton in the RVD and RVI processes in Ehrlich ascites tumor cells. Experimental Cell Research 1999;252:63–74. [PubMed: 10502400]
25. Hallows KR, Packman CH, Knauf PA. Acute cell-volume changes in anisotonic media affect F-actin content of HL-60 cells. American Journal of Physiology 1991;261:C1154–C1161. [PubMed: 1767817]
26. Thirone ACP, Speight P, Zulys M, Rotstein OD, Szaszi K, Pedersen SF, Kapus A. Hyperosmotic stress induces Rho/Rhokinase/LIM kinase-mediated cofilin phosphorylation in tubular cells: key role in the osmotically triggered F-actin response. American Journal of Physiology-Cell Physiology 2009;296:C463–C475. [PubMed: 19109524]
27. Tamma G, Klussmann E, Maric K, Aktories K, Svelto M, Rosenthal W, Valenti G. Rho inhibits cAMP-induced translocation of aquaporin-2 into the apical membrane of renal cells. American Journal of Physiology-Renal Physiology 2001;281:F1092–F1101. [PubMed: 11704560]
28. Hoffman GR, Nassar N, Cerione RA. Structure of the Rho family GTP-binding protein Cdc42 in complex with the multifunctional regulator RhoGDI. Cell 2000;100:345–356. [PubMed: 10676816]
29. Di Ciano-Oliveira, C.; Thirone, ACP.; Szaszi, K.; Kapus, A. Osmotic stress and the cytoskeleton: the R(h)ole of Rho GTPases. 2006. p. 257-272.
30. Ab JY, Shi GX, Shao Y, Dai G, Wei JN, Chang DC, Li CJ. Calmodulin bound to stress fibers but not microtubules involves regulation of cell morphology and motility. International Journal of Biochemistry & Cell Biology 2008;40:284–293. [PubMed: 17884685]
31. Satsu H, Manabe M, Shimizu M. Activation of Ca2+/calmodulin-dependent protein kinase II is involved in hyperosmotic induction of the human taurine transporter. Febs Letters 2004;569:123–128. [PubMed: 15225620]
32. Garciaperez A, Burg MB. Renal medullary organic osmolytes. Physiological Reviews 1991;71:1081–1115. [PubMed: 1924548]
33. Terubayashi H, Sato S, Nishimura C, Kador PF, Kinoshita JH. Localization of aldose and aldehyde reductase in the kidney. Kidney Int 1989;36:843–851. [PubMed: 2515341]
34. Witzmann FA, Fultz CD, Grant RA, Wright LS, Kornguth SE, Siegel FL. Differential expression of cytosolic proteins in the rat kidney cortex and medulla: preliminary proteomics. Electrophoresis 1998;19:2491–2497. [PubMed: 9820973]
35. Thedieck C, Kalbacher H, Kratzer U, Lammers R, Stevanovic S, Klein G. alpha B-crystallin is a cytoplasmic interaction partner of the kidney-specific cadherin-16. Journal of Molecular Biology 2008;378:145–153. [PubMed: 18343407]
36. Noda Y, Saburo HC, Katayama Y, Sasaki S. Identification of a multiprotein "motor" complex binding to water channel aquaporin-2. Biochem Biophys Res Commun 2005;330:1041–1047. [PubMed: 15823548]
37. Sharma M, Naslavsky N, Caplan S. A role for EHD4 in the regulation of early endosomal transport. Traffic 2008;9:995–1018. [PubMed: 18331452]
38. Blume JJ, Halbach A, Behrendt D, Paulsson M, Plomann M. EHD proteins are associated with tubular and vesicular compartments and interact with specific phospholipids. Exp Cell Res 2007;313:219–231. [PubMed: 17097635]
39. Cristia E, Amat C, Naftalin RJ, Moreto M. Role of vasopressin in rat distal colon function. J Physiol 2007;578:413–424. [PubMed: 17082233]

40. Wood ZA, Schroder E, Harris JR, Poole LB. Structure, mechanism and regulation of peroxiredoxins. Trends in Biochemical Sciences 2003;28:32–40. [PubMed: 12517450]

41. Dastoor Z, Dreyer JL. Potential role of nuclear translocation of glyceraldehyde-3-phosphate dehydrogenase in apoptosis and oxidative stress. J Cell Sci 2001;114:1643–1653. [PubMed: 11309196]

42. Dai RP, Yu FX, Goh SR, Chng HW, Tan YL, Fu JL, Zheng L, Luo Y. Histone 2B (H2B) expression is confined to a proper NAD+/NADH redox status. J Biol Chem 2008;283:26894–26901. [PubMed: 18682386]

43. Kultz D. Hyperosmolality triggers oxidative damage in kidney cells. Proceedings of the National Academy of Sciences of the United States of America 2004;101:9177–9178. [PubMed: 15199186]

44. Dastoor Z, Dreyer JL. Potential role of nuclear translocation of glyceraldehyde-3-phosphate dehydrogenase in apoptosis and oxidative stress. Journal of Cell Science 2001;114:1643–1653. [PubMed: 11309196]

45. Dai RP, Yu FX, Goh SR, Chng HW, Tan YL, Fu JL, Zheng L, Luo Y. Histone 2B (H2B) expression is confined to a proper NAD(+)/NADH redox status. Journal of Biological Chemistry 2008;283:26894–26901. [PubMed: 18682386]

46. Schmitz HD, Bereiter-Hahn J. Glyceraldehyde-3-phosphate dehydrogenase associates with actin filaments in serum deprived NIH 3T3 cells only. Cell Biol Int 2002;26:155–164. [PubMed: 11846445]

47. Sirover MA. Role of the glycolytic protein, glyceraldehyde-3-phosphate dehydrogenase, in normal cell function and in cell pathology. J Cell Biochem 1997;66:133–140. [PubMed: 9213215]

48. Arai H, Atomi Y. Chaperone activity of alpha B-crystallin suppresses tubulin aggregation through complex formation. Cell Structure and Function 1997;22:539–544. [PubMed: 9431459]

49. Yuasa-Kawada J, Suzuki R, Kano F, Ohkawara T, Murata M, Noda M. Axonal morphogenesis controlled by antagonistic roles of two CRMP subtypes in microtubule organization. Eur J Neurosci 2003;17:2329–2343. [PubMed: 12814366]

50. Beck KA, Nelson WJ. A spectrin membrane skeleton of the Golgi complex. Biochimica Et Biophysica Acta-Molecular Cell Research 1998;1404:153–160.

51. Cueille N, Blanc CT, Riederer IM, Riederer BM. Microtubule-associated protein 1B binds glyceraldehyde-3-phosphate dehydrogenase. J Proteome Res 2007;6:2640–2647. [PubMed: 17521179]

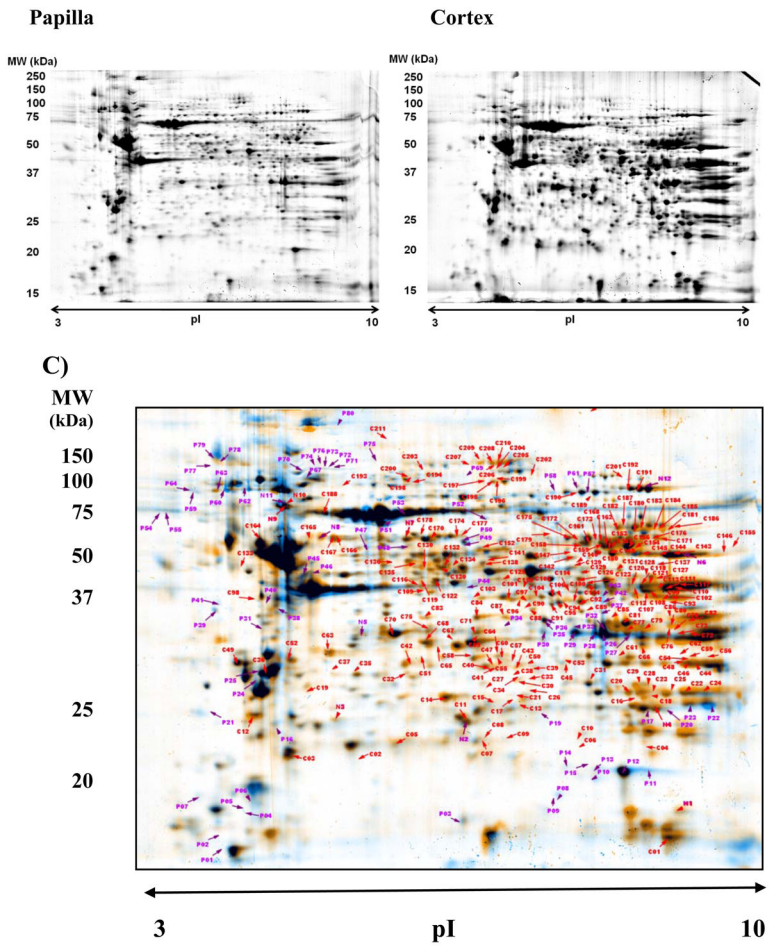

Figure 1.

Proteome maps of kidney regions A) Proteome map of renal papilla B) Proteome map of renal cortex C) Dual image overlay of papilla and cortex. Proteins significantly over-represented in papilla are labeled in purple; proteins significantly over-represented in cortex are labeled in red.

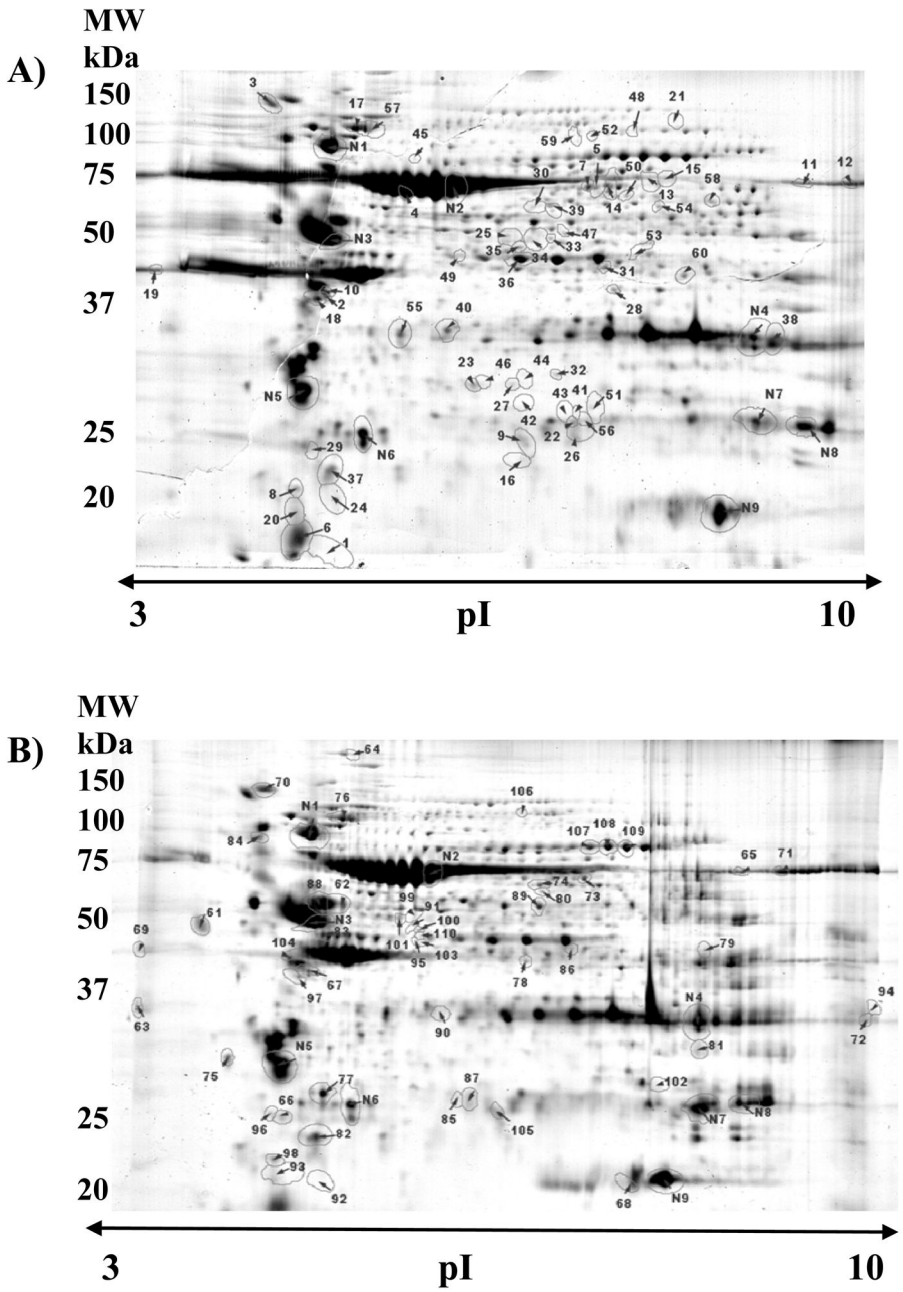

Figure 2.
Proteome Maps of Renal Papilla following A) Antidiuretic treatment and B) Diuretic treatment. Labeled proteins are differentially expressed relative to appropriate control group.

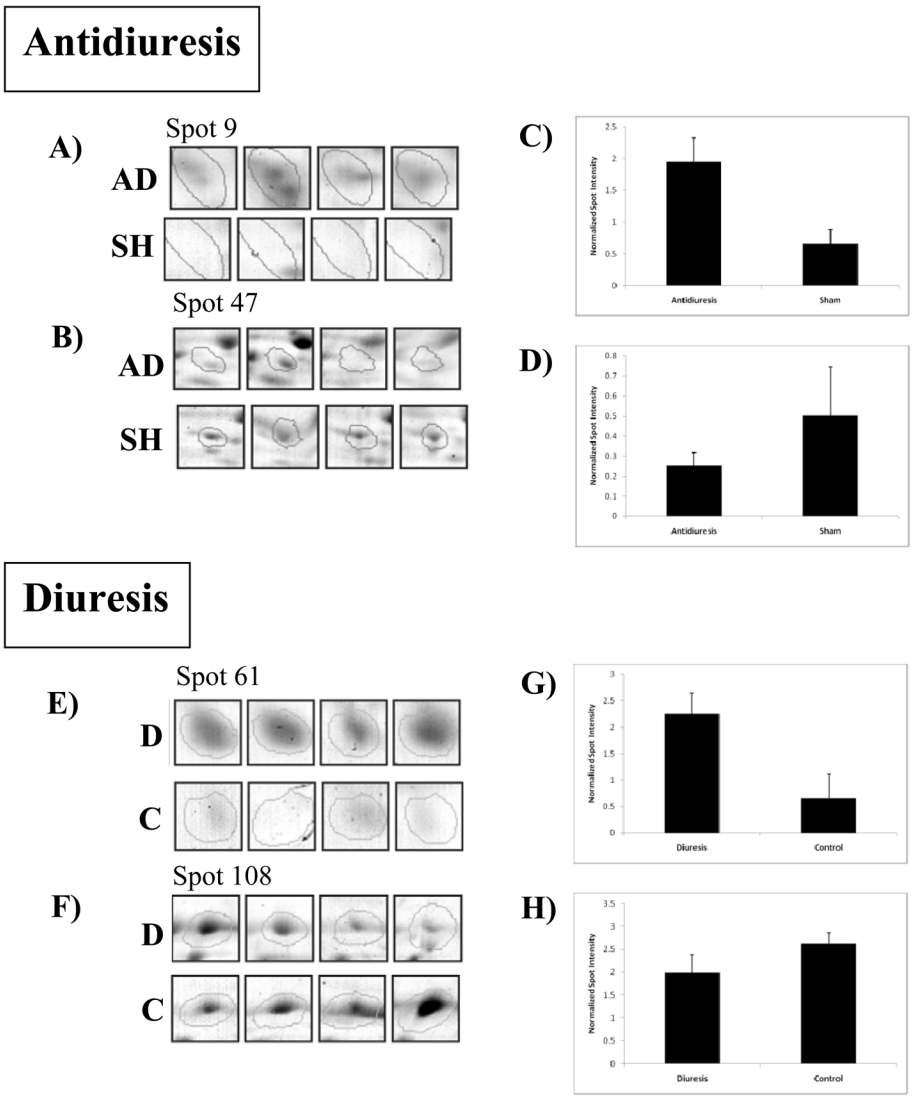

Figure 3.

Representative spot intensity quantification for differentially expressed proteins. 2D gel image close-up of replicates (n=4) for proteins A) up-regulated and B) down-regulated by antidiuresis (AD) relative to sham injection (SH). C) and D) show expression quantification based on CCB stain intensity of proteins shown in A) and B) respectively. Close-up of proteins E) up-regulated and F) down-regulated by diuresis (D) relative to control (C). G) and H) show the associated expression quantification.

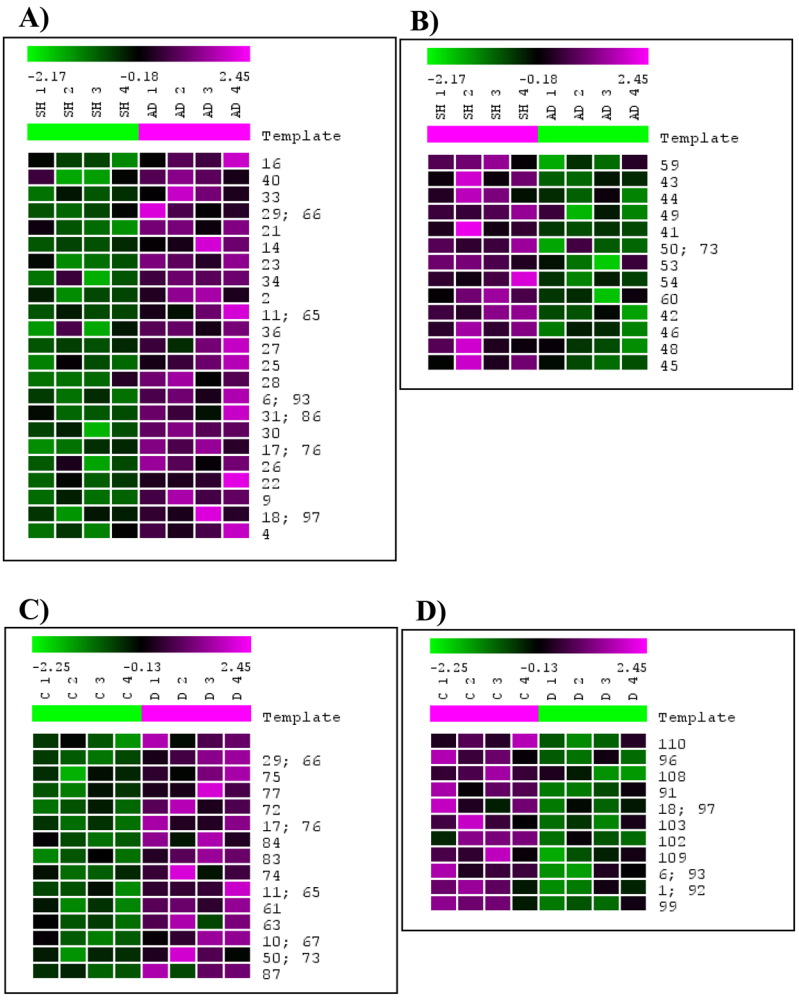

Figure 4.

Heat maps of proteins differentially expressed during osmolality treatment. Pink indicates high expression; green proteins are low while black proteins are similarly expressed between groups. A) proteins up-regulated during antidiuresis B) proteins down-regulated during antidiuresis C) proteins up-regulated during diuresis D) proteins down-regulated during diuresis. Pavlividis template matched expression changes significant at $p<0.05$.

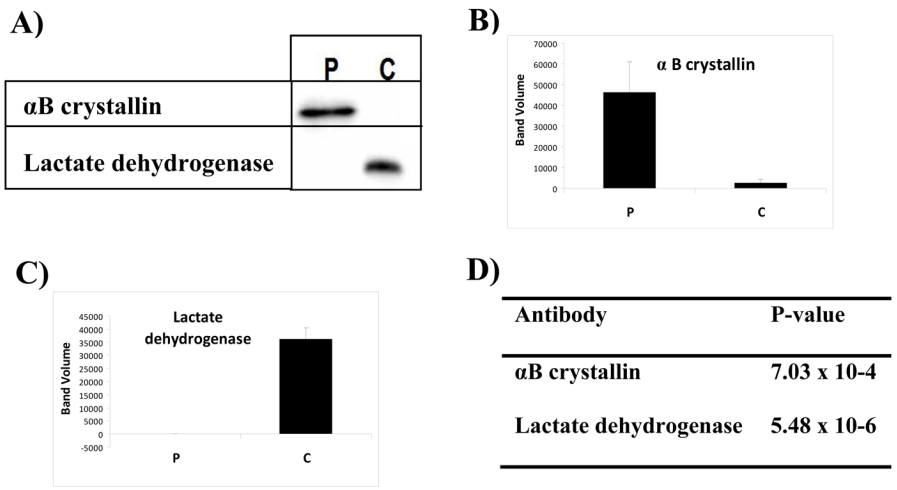

Figure 5.

Western blot confirmation of regional over-representation of αB crystallin and lactate dehydrogenase. A) Blot bands from papilla (P) and cortex (C). Quantification of band volume (n=6) for B) αB crystallin and C) lactate dehydrogenase D) p-values for comparisons of band volumes between regions.

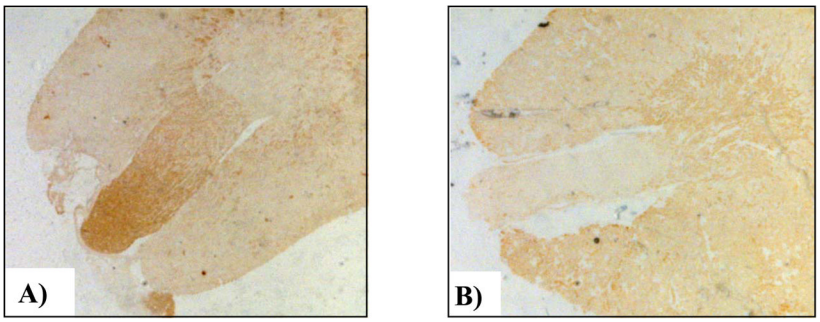

Figure 6.
Immunohistochemical confirmation of regional over-representation. Mouse kidney cross-sections were incubated with antibodies to detect A) αB crystallin or B) lactate dehydrogenase. Brown reaction product is present predominantly within A) the papilla or B) the cortex.

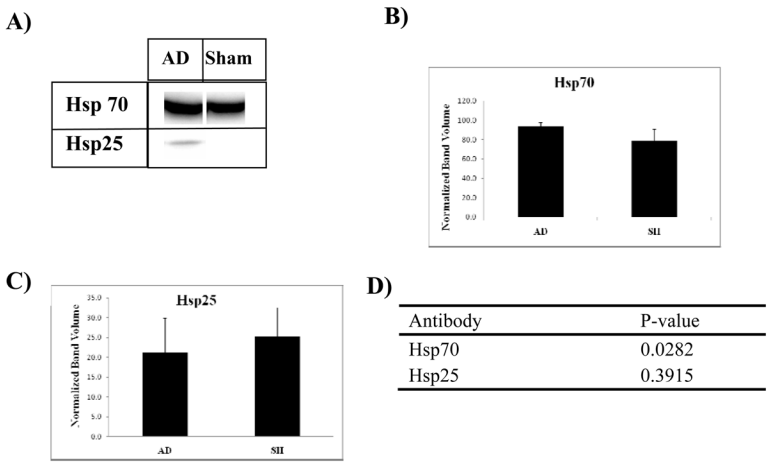

D)

Antibody	P-value
Hsp70	0.0282
Hsp25	0.3915

Figure 7.

Western blot confirmation of treatment induced expression of Hsp70 and Hsp25. A) Blot bands from antidiuretic (AD) and diuretic (D) mice. Quantification of band volume (n=4) for B) Hsp70 and C) Hsp25. D) p-values for comparisons of band volumes between treatments.

Table 1

Identified Proteins Over-Represented in the Renal Papilla

Spot No.	Protein Name	Accession Number	Score (MASCOT)	No. of Matched Peptides	Sequence Coverage (%)	pI	MW (kDa)	Ratio* P/C
03	ADP-ribosylation factor 1	ARF1_MOUSE	259	6	-	6.36	20610	5.27
07	Calmodulin	CALM_MOUSE	137	6	46	4.09	16696	6.40
10	Alpha crystallin B chain	CRYAB_MOUSE	333	10	40	6.76	20056	9.70
12	Alpha crystallin B chain	CRYAB_MOUSE	296	9	40	6.76	20056	6.56
13	Alpha crystallin B chain	CRYAB_MOUSE	238	8	33	6.76	20076	17.44
16	Rho GDP-dissociation inhibitor 2	GDIS_MOUSE	105	3	-	4.97	22894	3.07
17	Glutathione S-transferase Mu 2	GSTM2_MOUSE	410	14	-	7.3	25740	3.44
18	Hsp beta-1	HSPB1_MOUSE	97	5	22	6.12	23057	2.84
22	Glutathione S-transferase Mu 1	GSTM1_MOUSE	367	16	-	8.13	25936	3.41
23	Glutathione S-transferase Mu 1	GSTM1_MOUSE	294	12	-	8.13	25936	3.71
24	14-3-3 protein epsilon	1433E_MOUSE	262	9	41	4.63	29326	2.51
25	Tropomyosin alpha 3 chain	TPM3_MOUSE	328	14	60	4.68	32900	2.48
26	Aldose reductase	ALDR_MOUSE	263	9	32	6.71	36052	2.44
28	Aldose reductase	ALDR_MOUSE	97	-	-	6.79	35920	4.46
29	Aldose reductase	ALDR_MOUSE	231	6	-	6.79	35920	3.50
32	Aldose reductase	ALDR_MOUSE	301	8	-	6.79	35921	3.11
45	Actin	ACTB_MOUSE	99	5	11	5.29	42052	2.54
51	Serum Albumin	ALBU_MOUSE	606	14	34	5.75	70700	3.86
57	Serotransferrin	TRFE_MOUSE	464	21	25	6.94	78841	2.52
60	Heat shock protein 90-alpha	HS90A_HORSE	134	7	8	5	83445	5.25
67	Transitional endoplasmic reticulum ATPase	TERA_MOUSE	320	11	13	5.14	89950	2.17
70	Endoplasmin (GRP94)	ENPL_BOVIN	294	22	22	4.76	92654	2.70

*Expression is described as the ratio of that in the papilla to that in the cortex.

Table 2

Identified Proteins Over-Represented in the Renal Cortex

Spot No.	Protein Name	Accession Number	Score (MASCOT)	No. of Matched Peptides	Sequence Coverage (%)	pI	MW (kDa)	Ratio* C/P
12	Calbindin	CALB1_MOUSE	203	6	22	4.71	30072	3.08
20	Peroxiredoxin 5	PRDX5_MOUSE	108	6	33	9.1	22225	2.18
22	Electron transfer flavoprotein	ETFB_MOUSE	228	8	-	8.57	27521	3.48
25	Enoyl-CoA hydratase	ECHM_RAT	228	7	7	8.39	31895	3.49
26	Enoyl-CoA hydratase	ECHM_RAT	201	8	33	8.39	31895	4.13
31	Carbonic anhydrase 2	CAH2_MOUSE	160	6	21	6.52	29056	4.82
42	Ketohexokinase	KHK_MOUSE	218	7	30	5.81	33300	4.21
55	Δ-3,5- Δ-2,4-dienoyl-CoA isomerase	ECH1_MOUSE	90	7	-	7.6	36437	4.69
62	Malate dehydrogenase	MKHC_MOUSE	241	12	29	6.16	36659	7.96
63	Aspartoacylase 2	ACY3_MOUSE	140	6	37	5.3	35720	2.21
69	Fructose-1,6-bisphosphatase	F16P_MOUSE	132	10	-	6.18	37157	2.19
70	L-lactate dehydrogenase B chain	LDHB_MOUSE	331	13	-	5.7	36703	2.13
75	L-lactate dedydrogenase B chain	LDHB_RAT	176	7	-	5.7	36743	2.16
77	Alcohol dehydrogenase	AK1A_MOUSE	185	9	-	6.87	36660	2.70
79	Hydroxyacid oxidase 3	HAOX3_MOUSE	93	8	-	7.55	39131	3.44
80	Quinone oxidoreductase	QOR_MOUSE	383	14	56	8.18	35531	4.80
82	Fructose-bisphosphate aldolase B	ALDOB_MOUSE	278	7	-	8.53	39807	4.39
84	L-lactate dehydrogenase B chain	LDHB_MOUSE	231	9	-	5.7	36743	5.59
91	Sorbitol dehydrogenase	DHSO_MOUSE	362	9	-	6.6	40636	3.88
93	Acetyl-CoA acetyltransferase	THIL_MOUSE	127	8	26	8.71	45129	3.08
95	Sorbitol dehydrogenase	DHSO_MOUSE	245	13	-	6.6	40636	3.95
99	Acetyl-CoA acetyltransferase	THIL_MOUSE	321	10	38	8.71	45129	4.49
105	Isovaleryl-CoA dehydrogenase	IVD_HUMAN	186	4	13	8.45	46803	2.49
107	Acyl-CoA dehydrogenase	ACADM_MOUSE	172	14	36	8.6	46908	3.52
108	Acyl-CoA dehydrogenase	ACADM_MOUSE	300	15	17	8.6	46908	3.84
117	Argininosuccinate synthase	ASSY_MOUSE	208	13	24	8.36	46840	2.65
119	NDRG1 protein	NDRG1_MOUSE	148	4	24	5.69	43437	4.10
122	Ornithine aminotransferase	OAT_MOUSE	502	17	52	6.19	48723	2.16

Spot No.	Protein Name	Accession Number	Score (MASCOT)	No. of Matched Peptides	Sequence Coverage (%)	pI	MW (kDa)	Ratio* C/P
126	Isocitrate dehydrogenase	IDHC_RAT	145	8	15	6.53	47047	2.58
127	Fumarate hydratase	FUMH_MOUSE	109	7	19	9.12	54564	3.37
127	Glutamine synthetase	GLNA_RAT	174	9	21	6.64	42982	3.37
129	Glycine amidinotransferase	GATM_MOUSE	151	12	30	8.0	48779	3.69
130	Alpha enolase	ENOA_MOUSE	99	9	-	6.36	47322	2.26
135	Dihydrolipoyllisine-residue succinyltransferase component of 2-oxoglutarate dehydrogenase	ODO2_RAT	175	6	-	8.17	47668	2.77
138	Alpha enolase	ENOA_MOUSE	526	20	-	6.81	47007	3.19
143	ATP synthase alpha chain	ATPA_MOUSE	855	16	35	9.16	59828	2.23
144	ATP synthase alpha chain	ATPA_MOUSE	819	13	29	9.16	59828	4.14
148	Glutamate dehydrogenase 1	DHE3_MOUSE	275	14	17	8.05	61640	3.85
153	Methylmalonate-semialdehyde dehydrogenase	MMSA_BOVIN	399	9	24	8.3	58482	2.77
154	Glutamate dehydrogenase 1	DHE3_MOUSE	274	15	18	8.05	61640	3.29
156	Methylmalonate-semialdehyde dehydrogenase	MMSA_RAT	310	11	15	8.47	58227	2.68
157	Methylmalonate-semialdehyde dehydrogenase	MMSA_RAT	104	8	12	8.47	58227	4.00
162	Succinyl-CoA:3-ketoacid-CoA transferase 1	SCOT_MOUSE	293	11	11	8.73	56352	3.05
164	Protein disulfide-isomerase	PDIA1_MOUSE	631	14	32	4.79	57507	2.27
170	Protein disulfide-isomerase A3	PDIA3_MOUSE	128	13	2	5.98	57042	2.61
175	Dihydrolipoyl dehydrogenase	DLDH_MOUSE	182	11	23	7.99	54751	3.49
180	Δ-1-pyroline-5-carboxylate dehydrogenase	AL4A1_MOUSE	230	9	-	8.58	62228	2.25
190	Aconitate hydratase	ACON_MOUSE	666	32	-	8.08	86151	2.48
191	Aconitate hydratase	ACON_MOUSE	520	19	32	8.08	86151	3.32
192	Aconitate hydratase	ACON_MOUSE	123	12	15	8.08	86151	2.22
210	Pyruvate carboxylase	PYC_MOUSE	103	13	11	6.25	130344	2.72

*Expression is described as the ratio of that in the cortex to that in the papilla.

Table 3

Identified Proteins Differentially Expressed During Antidiuresis

Spot No.	Protein Name	Accession Number	Score (MASCOT)	No. of Matched Peptides	Sequence Coverage (%)	pI	MW (kDa)	Fold Change	p-value
3	Cadherin-16	CAD16_MOUSE	189	8	12	4.53	90,203	3.52	0.063
4	HSP 70	HS71B_MOUSE	341	26	48	5.53	70,321	3.46	0.014
5	EH domain-containing protein	EHD4_MOUSE	243	16		6.33	61670	3.31	0.057
9	Abhydrolase-domain containing protein 14B	ABHEB_MOUSE	190	7	38	5.82	22,551	2.96	0.001
17	Alpha-actinin-4	ACTN4_RAT	374	30	47	5.27	105,306	2.24	0.002
19	Actin, cytoplasmic	ACTB_HORSE	319	14	40	5.29	42,052	2.03	0.078
22	Peroxiredoxin-6	PRDX6_MOUSE	330	11	49	5.71	24,969	1.93	0.042
36	Alpha-enolase	ENOA_MOUSE	290	12	33	6.37	47,453	1.45	0.046
37	Peroxiredoxin-2	PRDX2_MOUSE	204	8	41	5.2	21,936	1.41	0.072
38	Glyceraldehyde-3-phosphate dehydrogenase	G3P_MOUSE	128	11	38	8.44	36,072	1.41	0.053
40	L-lactate dehydrogenase B chain	LDHB_MOUSE	227	11	52	5.7	36,834	1.27	0.044
41	HSP beta-1	HSPB1_MOUSE	398	17	57	6.12	23,057	−4.76	0.045
43	HSP beta-1	HSPB1_MOUSE	327	10	44	6.12	23,057	−2.63	0.035
47	T-complex protein 1 subunit beta	TCPB_MOUSE	406	21	55	5.97	57,783	−1.96	0.097
49	Alpha-enolase	ENOA_MOUSE	261	10	29	6.37	47,453	−1.96	0.031
53	Alpha-enolase	ENOA_MOUSE	670	18	47	6.37	47,453	−1.61	0.036
55	Guanine nucleotide- binding protein	GBB2_RAT	170	11	27	5.6	38,048	−1.52	0.073
60	Long-chain specific acyl-CoA dehydogenase	ACADL_PIG	199	14	31	6.96	48,326	−1.27	0.026

Table 4

Identified Proteins Differentially Expressed During Diuresis

Spot No.	Protein Name	Accession Number	Score (MASCOT)	No. of Matched Peptides	Sequence Coverage (%)	pI	MW (kDa)	Fold Change	p-value
61	Antithrombin-III	ANT3-MOUSE	428	26	54	6.1	52,484	3.43	0.002
62	Tubulin alpha-1C chain	TBA1C_MOUSE	135	7	31	4.96	50,562	3.27	0.093
63	Aldose reductase	ALDR_MOUSE	167	12	37	6.71	36,052	3.18	0.047
64	Spectrin alpha chain	SPTA2_RAT	218	31		5.2	285261	2.94	0.082
68	Alpha-crystallin B chain	CRYAB_MOUSE	394	17	78	6.76	20,056	2.14	0.104
69	Actin, cytoplasmic	ACTB_HORSE	319	14	40	5.29	42,052	2.10	0.094
74	Dihydropyrimidinase-related protein 2	DPYL2_MOUSE	250	13	33	5.95	62,638	1.88	0.044
75	Acidic leucine-rich nuclear phosphoprotein	AN32A_MOUSE	381	15	40	3.99	28,691	1.83	0.030
76	Alpha-actinin-4	ACTN4_RAT	374	30	47	5.27	105,306	1.76	0.005
77	Rho GDP-dissociation inhibitor 1	GDIR1_MOUSE	409	14	65	5.12	23,450	1.66	0.026
79	Fumarate hydratase	FUMH_MOUSE	153	8	17	9.12	54,564	1.64	0.063
82	Peroxiredoxin-2	PRDX2_MOUSE	204	8	41	5.2	21,936	1.40	0.073
88	Tubulin alpha-1B chain	TBA1B_CIGR	620	19	52	4.94	50,804	1.28	0.067
93	Major urinary protein 2	MUP2_MOUSE	407	10	49	5.04	20,935	−2.50	0.040
96	Translationally-controlled tumor protein	TCTP_RAT	235	9	44	4.76	19,564	−2.27	0.016
101	Fibrinogen gamma chain	FIBG_MOUSE	134	11	30	5.54	50,044	−1.70	0.072
104	40S Ribosomal Protein SA	RSSA_MOUSE	410	12	48	4.8	32,931	−1.47	0.080
105	Abhydrolase domain-containing protein 14B	ABHEB_MOUSE	133	7	38	5.82	22,551	−1.43	0.054
107	Serotransferrin	TRFE_MOUSE	326	24	30	6.94	78,841	−1.35	0.093
108	Serotransferrin	TRFE_MOUSE	437	24	32	6.94	78,841	−1.33	0.020
109	Serotransferrin	TRFE_MOUSE	272	23	36	6.94	78,841	−1.32	0.041

Table 5

PANTHER Analysis of Renal Papilla and Cortex

Kidney Region		No. Identified Proteins Involved	P-value*
Papilla	**Biological Process**		
	Protein folding	3	0.00951
	Molecular Function		
	Chaperone	3	0.0275
Cortex	**Biological Process**		
	Carbohydrate metabolism	16	7.39 × 10–17
	Amino acid metabolism	8	1.33 × 10–8
	Tricarboxylic acid pathway	4	1.38 × 10–5
	Other carbohydrate metabolism	4	0.000151
	Other carbon metabolism	4	0.000552
	Nitrogen metabolism	2	0.00659
	Glycolysis	3	0.0066
	Fatty acid metabolism	4	0.0198
	Other metabolism	5	0.0241
	Electron Transport	4	0.0247
	Molecular Function		
	Dehydrogenase	14	2.17 × 10–18
	Oxidoreductase	16	1.98 × 10–15
	Lyase	6	1.58 × 10–6
	Hydratase	2	0.0381

* p-value for significance of identified proteins over-represented in papilla or cortex when compared to the entire mouse genome (NCBI).

Table 6

Biological processes and molecular functions significantly altered by antidiuretic and diuretic treatment as determined by PANTHER Analysis. The list of proteins identified as increased during antidiuresis was combined with the list of proteins that decreased during diuresis to create the group termed ‘related to increased urine osmolality’. Proteins identified as increasing or decreasing during antidiuresis form the second group ‘change with antidiuresis’

Protein Group	Altered Processes and Functions	No. Identified Proteins Involved	p-value
Related to Increased Urine Osmolality	**Biological Process**		
	Immunity and defense	7	0.00206
	Antioxidation and free radical removal	2	0.0402
	Glycolysis	2	0.0296*
	Molecular Function		
	Peroxidase	2	0.0248
Change with Antidiuresis	**Biological Process**		
	Protein folding	3	0.015
	Antioxidation and free radical removal	2	0.0311
	Molecular Function		
	Chaperone	3	0.0035
	Oxidoreductase	4	0.0128
	Peroxidase	2	0.0192

* p-value for list of proteins that increase with antidiuresis without those that decrease with diuresis; the combined list generates a p-value of 0.0727.